Report

Cell Reports

The Phosphate Exporter *xpr1b* Is Required for Differentiation of Tissue-Resident Macrophages

Graphical Abstract

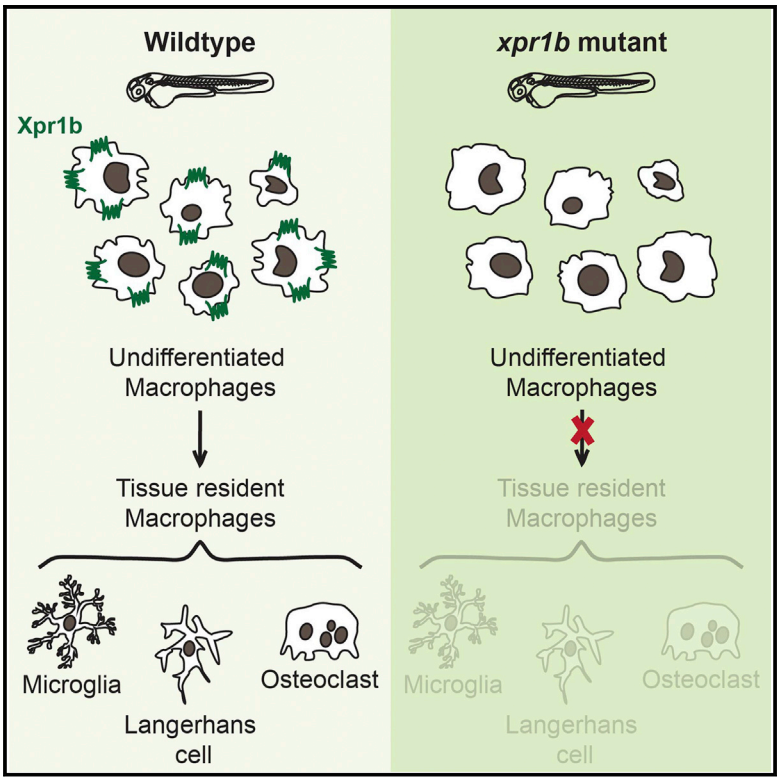

Highlights

xpr1b phosphate exporter is required for tissue macrophage differentiation in vivo

xpr1b acts autonomously in macrophages

Xpr1 zygotic function is dispensable for viability of the embryo and early larva

Authors

Ana M. Meireles, Celia E. Shiau, ..., David M. Kingsley, William S. Talbot

Correspondence

william.talbot@stanford.edu

In Brief

XPR1 is the only known metazoan exporter for inorganic phosphate, a crucial ion necessary for bone mineralization and diverse cellular activities. Meireles et al. now identify null mutations in *xpr1a* and *xpr1b*, the zebrafish orthologs of human XPR1. Zebrafish *xpr1b* mutants lack microglia and other tissue-resident macrophage populations but display no gross developmental defects, and *xpr1a;xpr1b* double mutants have a similar phenotype. This genetic analysis reveals a specific role for Xpr1b in the differentiation of tissue macrophages.

Meireles et al., 2014, Cell Reports 8, 1659–1667
September 25, 2014 ©2014 The Authors
http://dx.doi.org/10.1016/j.celrep.2014.08.018

Cell Reports
Report

The Phosphate Exporter *xpr1b* Is Required for Differentiation of Tissue-Resident Macrophages

Ana M. Meireles,[1] Celia E. Shiau,[1] Catherine A. Guenther,[1,2] Harwin Sidik,[1] David M. Kingsley,[1,2] and William S. Talbot[1,*]
[1]Department of Developmental Biology, Stanford University School of Medicine, Stanford, CA 94305, USA
[2]Howard Hughes Medical Institute, Stanford University School of Medicine, Stanford, CA 94305, USA
*Correspondence: william.talbot@stanford.edu
http://dx.doi.org/10.1016/j.celrep.2014.08.018

SUMMARY

Phosphate concentration is tightly regulated at the cellular and organismal levels. The first metazoan phosphate exporter, XPR1, was recently identified, but its in vivo function remains unknown. In a genetic screen, we identified a mutation in a zebrafish ortholog of human XPR1, *xpr1b*. *xpr1b* mutants lack microglia, the specialized macrophages that reside in the brain, and also displayed an osteopetrotic phenotype characteristic of defects in osteoclast function. Transgenic expression studies indicated that *xpr1b* acts autonomously in developing macrophages. *xpr1b* mutants display no gross developmental defects that may arise from phosphate imbalance. We constructed a targeted mutation of *xpr1a*, a duplicate of *xpr1b* in the zebrafish genome, to determine whether Xpr1a and Xpr1b have redundant functions. Single mutants for *xpr1a* were viable, and double mutants for *xpr1b;xpr1a* were similar to *xpr1b* single mutants. Our genetic analysis reveals a specific role for the phosphate exporter Xpr1 in the differentiation of tissue macrophages.

INTRODUCTION

Macrophages are a highly diverse population of immune cells present in virtually all tissues of vertebrates. Macrophages are important for not only phagocytosis and immune system regulation but also tissue homeostasis and development (Davies et al., 2013; Wynn et al., 2013). For example, besides their well-known role in the immune defense of the CNS, microglial cells (brain-resident macrophages) are also important for clearance of cellular debris and regulating neuronal connectivity (Paolicelli et al., 2011; Peri and Nüsslein-Volhard, 2008; Ransohoff and Cardona, 2010; Schafer et al., 2012). Similarly, osteoclasts (bone-resorbing macrophages) are essential for correct bone development, bone remodelling in adults, and mineral homeostasis at the organismal level. Mice that are devoid of osteoclasts develop osteopetrosis, a condition characterized by abnormal bone structure and altered hematopoiesis (Begg et al., 1993; Pollard, 1997). Despite the importance of tissue macrophages, the mechanisms that control the development and dedicated functions of tissue macrophages are not well understood.

Inorganic phosphate (Pi) is a crucial ion necessary for bone mineralization and diverse cellular activities, because it forms an integral part of membrane phospholipids, nucleic acids, and ATP. Furthermore, phosphate has an important role in many signaling pathways involving kinases and phosphatases (Biber et al., 2013; Forster et al., 2013). SLC34 and SLC20 are transporters that define two classes of molecules that import phosphate into cells. SLC34 family members are expressed and localized in the apical membrane of enterocytes (NPT2b/SLC34A2) and epithelial cells of the proximal tubule in the kidney (NPT2a/SLC34A1). Members of SLC20 family are ubiquitously expressed and are considered to be suppliers of phosphate for cellular metabolism and bone mineralization (Biber et al., 2013; Forster et al., 2013). Although the existence of a dedicated phosphate exporter has long been hypothesized, the first metazoan phosphate exporter, XPR1, was only recently identified (Giovannini et al., 2013).

XPR1 is a highly conserved multipass transmembrane protein originally identified as a receptor for xenotropic and polytropic murine retroviruses (Battini et al., 1999; Tailor et al., 1999; Yang et al., 1999). XPR1 possesses two characteristic protein domains: SPX (named after the proteins Syg1, Pho81, and XPR1) and EXS (named after the proteins ERD, XPR1 and Syg1). The SPX domain is conserved throughout evolution and present in many yeast and plant proteins involved in phosphate homeostasis (Secco et al., 2012a, 2012b). The SPX domain of XPR1 is dispensable for phosphate export and viral infection (Giovannini et al., 2013; Wege and Poirier, 2014). Because overexpression of XPR1 or of a truncated form containing the SPX domain leads to an increase in intracellular cyclic AMP levels (Vaughan et al., 2012), and because XPR1 interacts with the Gβ subunit of the G protein trimer, this protein has also been classified as an atypical G protein-coupled receptor (Vaughan et al., 2012). Despite the evidence for a role in phosphate export and its potential role as a transmembrane receptor, XPR1 may also have other activities, and there is little understanding of its function in vivo.

xpr1a and *xpr1b* are the zebrafish orthologs of XPR1. In this study, we show that the phosphate exporter *xpr1b* acts specifically in macrophages to promote the differentiation and establishment of several tissue-resident macrophage populations. *xpr1b* mutants lack microglia and also have a reduction in the number and complexity of Langerhans cells. Furthermore, we

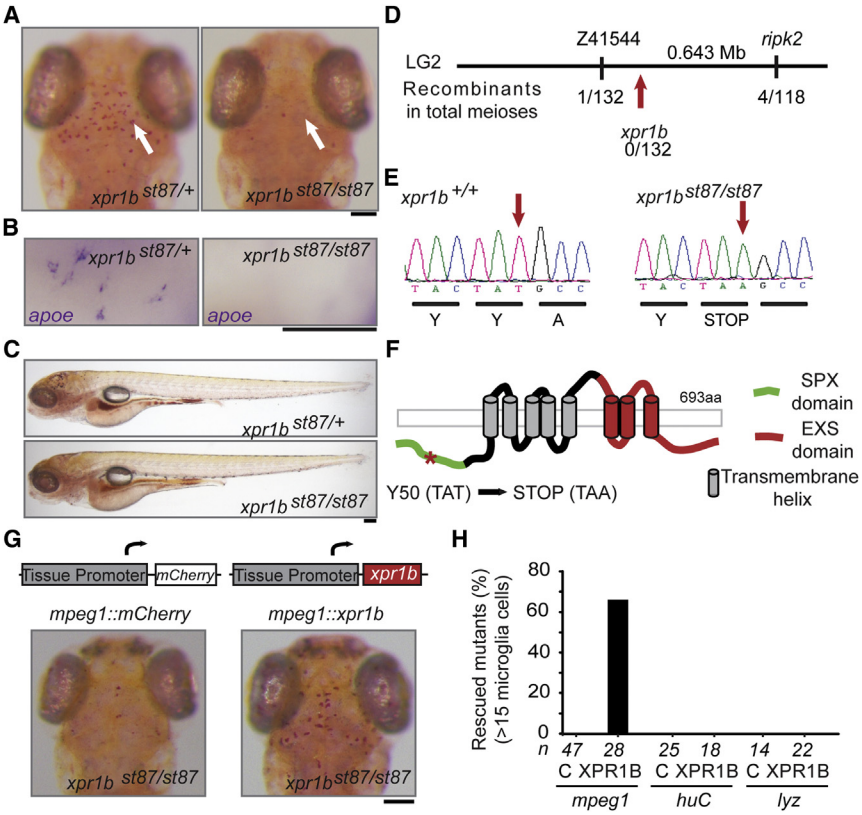

Figure 1. *xpr1b* Is Required Autonomously in Macrophages for Microglia Development

(A) The 5 dpf zebrafish larvae were stained with the microglial vital marker neutral red (Herbomel et al., 2001). Left panel shows the dorsal view of *xpr1b* heterozygous larva with microglia (arrow) in the optic tectum.

(B) Whole-mount in situ hybridization at 5 dpf reveals the expression of the microglial marker *apoe* in *xpr1b* heterozygous larva, but not in *xpr1b* mutants.

(C) Lateral view of neutral red-stained heterozygous and homozygous mutants shows normal whole-animal morphologies at 5 dpf.

(D) Schematic representation of the *st87* locus.

(E) Chromatogram depicts the lesion (arrow) in the coding sequence of *xpr1b*.

(F) Graphical representation of the domain structure of Xpr1 and the location of the *st87* lesion (asterisk).

(G) Diagram represents the transgenic constructs driving the expression of *mcherry* reporter or wild-type *xpr1b* under the control of macrophage (*mpeg1*), neurons (*huC*), or neutrophils (*lyz*) tissue promoters. Below are representative images of neutral red-stained *xpr1b* mutant fish expressing *mcherry* (left) or *xpr1b* (right) under the macrophage lineage-specific promoter. Microglia are present only when *xpr1b* is expressed under the *mpeg1* promoter.

(H) Graph shows the percentage of mutants rescued by different tissue-specific promoters. The number of embryos analyzed for each condition, *mCherry* (C) or *xpr1b*, is shown below.

Scale bar, 50 μm. See also Figure S1.

demonstrate that *xpr1b* mutants have profound defects in bone architecture characteristic of osteoclast disruption. Additionally, our genetic analysis of *xpr1a*, the only additional zebrafish paralog of *xpr1b*, showed that *xpr1a* mutants had no defects in microglia formation and that *xpr1b; xpr1a* double mutants are phenotypically similar to *xpr1b* mutants. Thus, our genetic analysis provides evidence that the macrophage lineage is particularly sensitive to alterations in Xpr1 function.

RESULTS

Genetic Screen Identifies *xpr1b* as a Regulator of Macrophage Development

We conducted a genetic screen for N-ethyl-N-nitrosourea (ENU)-induced mutations causing abnormalities in microglia, using the vital dye neutral red, a previously reported marker of macrophages and microglia in zebrafish (Herbomel et al., 2001). This screen identified *xpr1b*^{st87} as a mutation that severely reduced the number of neutral red-labeled microglia (Figures 1A). At 5 days postfertilization (dpf), homozygous *xpr1b*^{st87} mutant larvae lacked expression of the microglial marker *apolipoproteine* (*apoe*) (Herbomel et al., 2001; Peri and Nüsslein-Volhard, 2008) (Figure 1B) but were otherwise morphologically indistinguishable from wild-type and heterozygous siblings (Figure 1C). High-resolution genetic mapping placed the *xpr1b*^{st87} mutation in a 0.64 Mb region of linkage group 2 (LG2) that contains the *xpr1b* gene (Figure 1D). Xpr1b shares 79% identity and 87% similarity with the human XPR1 protein, which was originally identified as a retroviral receptor (Battini et al., 1999; Tailor et al., 1999; Yang et al., 1999) and has been recently characterized as an inorganic phosphate exporter (Giovannini et al., 2013). Sequence analysis of *xpr1b*^{st87} mutants identified a T to A transversion that introduces a premature stop codon near the 5′ end of *xpr1b* open reading frame (Figure 1E). All *xpr1b*^{st87} mutants analyzed were homozygous for this lesion (n = 80). To obtain additional evidence that *xpr1b* is disrupted by the *xpr1b*^{st87} mutation, we rescued the mutants by injecting synthetic mRNA encoding wild-type *xpr1b*. Injection of 200 pg of *xpr1b* mRNA into *xpr1b*^{st87} mutants rescued the microglia phenotype (Figure S1A). Furthermore, we also generated mutations in *xpr1b* using sequence-specific transcription activator-like effector (TALE) nucleases (Sanjana et al., 2012; Christian et al., 2010). We isolated two frameshift mutations, namely *xpr1b*^{st89} and *xpr1b*^{st90}. Both mutations failed to complement *xpr1b*^{st87}, and homozygous *xpr1b*^{st89} and *xpr1b*^{st90} mutants also lacked microglial cells (Figure S1B). Taken together, the mapping, analysis of two other mutant alleles, and rescue experiments demonstrate that *xpr1b*^{st87} is a loss-of-function mutation in the *xpr1b* gene.

xpr1b Is Required Autonomously in Macrophages for Microglia Development

To test whether Xpr1b is required autonomously in the macrophage lineage or in other cell types, we employed a transgenic rescue strategy. Coding sequences for *xpr1b* or the reporter

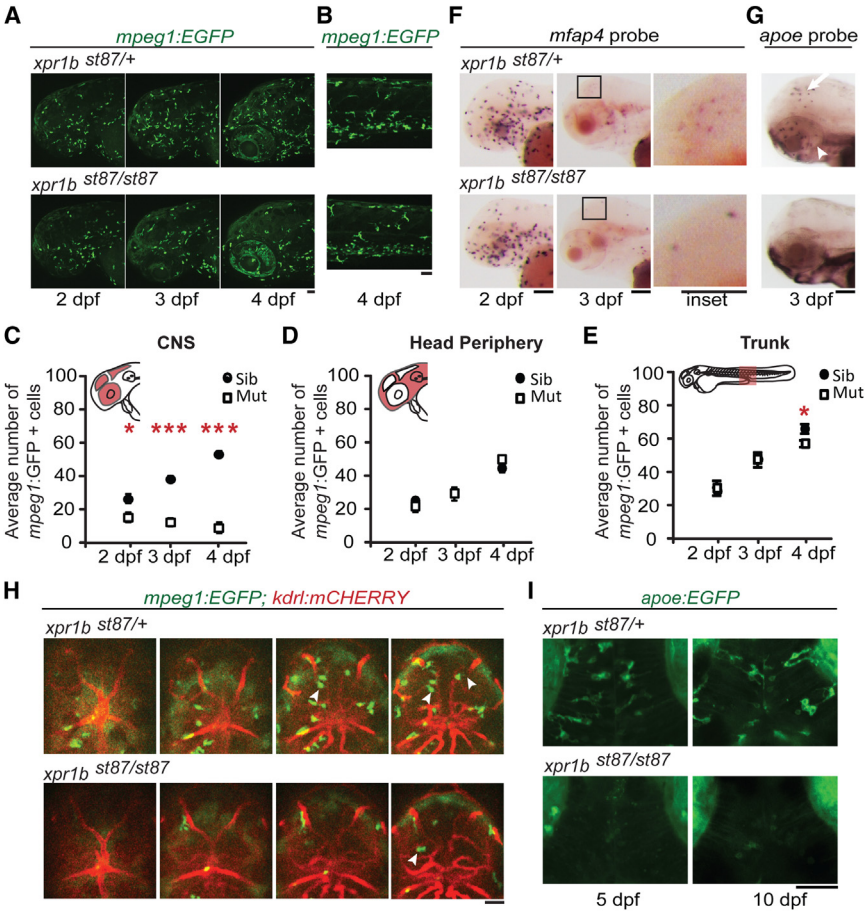

Figure 2. *xpr1b* Is Required for Brain Colonization by Microglial Progenitors

(A and B) Representative z-projections of *mpeg1:EGFP*-labeled cells at 2–4 dpf in the head (A) or 4 dpf in the trunk (B), in heterozygous larvae (top panel), or in *xpr1b* mutants (lower panel).

(C–E) Graphs show the average number of *mpeg1:EGFP*-positive cells in the highlighted region of fish schematics: CNS (eye, midbrain and hindbrain) (C), head periphery (D), and trunk (E). *xpr1b* mutants show a reduction in the average number of macrophages in the CNS region starting at 2 dpf. Error bars show SEM. Statistical significance was determined by paired two-tailed Student's test (*$p \leq 0.05$, **$p \leq 0.01$, ***$p \leq 0.001$; 2 dpf: mutants n = 7, siblings n = 16; 3 dpf: mutants n = 6, siblings n = 16; 4dpf: mutants n = 4, siblings n = 9).

(F) Whole-mount in situ hybridization at 2 and 3 dpf shows *mfap4*+ macrophages in the brain of wild-type heterozygous (top panel) larva, but not in *xpr1b* mutants (lower panel).

(G) Whole-mount in situ hybridization at 3 dpf shows *apoe*+ microglia in the brain of wild-type heterozygous (top panel) larva, but not in *xpr1b* mutants (lower panel).

(H) Serial single-plane images of stable transgenic fish expressing the macrophage marker *mpeg1:EGFP* and the vasculature marker *kdrl:mCHERRYCAAX*. Images show extensive penetration of macrophages into the brain of wild-type heterozygous fish (top panels) and only a few in *xpr1b* mutants (lower panels) (arrowheads indicate macrophages).

(I) z stack images of stable transgenic fish expressing the microglia marker *apoe:EGFP*. Images show microglia cells with processes in wild-type fish at 5 and 10 dpf (top panels), whereas no microglia cells are present in *xpr1b* mutants, even at 10 dpf (right panel).

Scale bar, 50 μm. See also Figures S2 and S3 and Movies S1, S2, S3, and S4

mCherry were expressed under the control of cell-specific regulatory elements that drive expression in neurons (*elavl3/huC*), neutrophils (*lyz*), or macrophages (*mpeg1*) as previously described (Shiau et al., 2013). Transient Tol2-mediated expression of the wild-type *xpr1b* gene under the control of *mpeg1* regulatory elements rescued microglia (>15 cells/embryo) in 67% of *xpr1b* mutants (n = 28). There was no significant rescue of microglia when *xpr1b* gene was expressed in other cell types or by expression of the *mCherry* coding sequence in any cell type (Figures 1G and 1H). These data indicate that *xpr1b* is required in the macrophage lineage for normal microglia development.

Brain Colonization of Microglia Is Disrupted in *xpr1b* Mutants

Microglia derive from a subset of primitive macrophages that migrate from the yolk sac into the brain, where they differentiate as microglia during embryogenesis (Ginhoux et al., 2010; Herbomel et al., 2001). To define the role of *xpr1b* during microglia development, we analyzed the macrophage lineage from the formation of primitive macrophages to differentiation of microglia (1–5 dpf). The markers *mfap4* (microfibrillar-associated protein 4; Zakrzewska et al., 2010) and *mpeg1:EGFP* (macrophage expressed gene 1; Ellett et al., 2011) are expressed in macrophages and microglia after they begin to differentiate at 60 hpf. Using these markers, we detected no difference in the number or distribution of macrophages up to 24 hpf (A.M.M., unpublished data). At 2 dpf, however, the number of *mpeg1:EGFP*-positive cells within the CNS (eye, midbrain, and hindbrain) was slightly but significantly reduced in *xpr1b* mutants (Figures 2A and 2C). This reduction became more apparent as development progressed, so that wild-type larvae had approximately 50 *mpeg1:EGFP*-positive microglia/per field of view at 4 dpf, compared to only about 14 in *xpr1b* mutants (Figures 2A and 2C).

We sought to determine whether the reduction in microglia in *xpr1b* mutants reflected an overall reduction of the precursor macrophage population. In contrast to microglia, there was no significant reduction in the number of *mpeg1:EGFP*-labeled macrophages in non-CNS locations of the head of *xpr1b* mutants at 2 dpf, 3 dpf, or 4 dpf (Figures 2A and 2D). Similarly, the number and distribution of *mpeg1:EGFP*-labeled macrophages in the trunk region of mutant larvae remained comparable to wild-type up to 4 dpf, although a slight reduction was

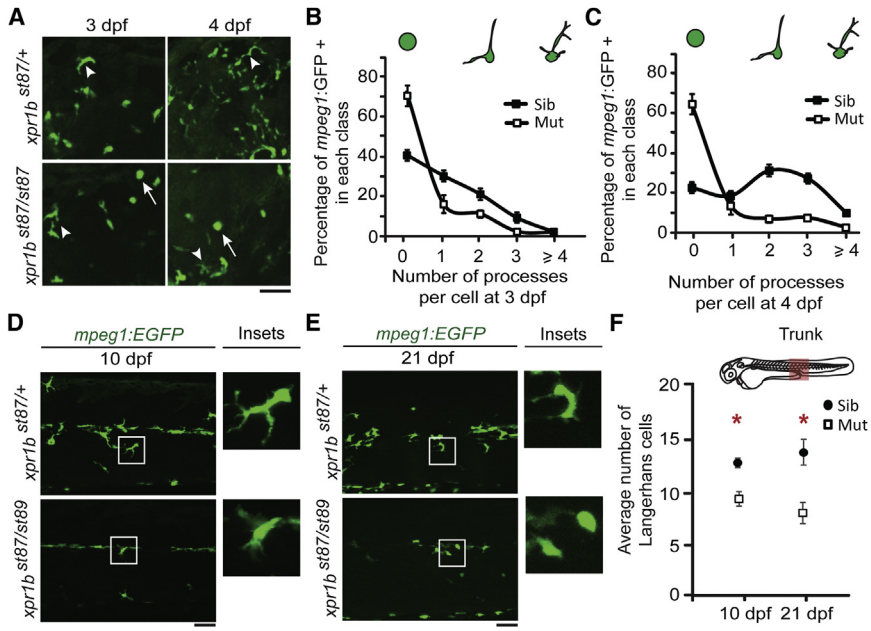

Figure 3. *xpr1b* Is Required for Differentiation of Microglia and Langerhans Cells

(A) Representative z stack images of the head region of stable *mpeg1:EGFP* transgenic fish at 3 and 4 dpf. In wild-type heterozygous fish, macrophages display an array of morphologies from rounded (arrows) to multiple process-bearing cells (arrowhead). In contrast, *xpr1b* mutants display a more restricted array of morphologies.

(B and C) Graphs show the percentage of *mpeg1:EGFP*-positive cells that contain 0, 1, 2, 3, or 4 or more processes at 3 dpf (B) or 4 dpf (C) (3 dpf siblings: n = 6, mutants n = 5; 4 dpf siblings: n = 4, mutants n = 4).

(D and E) Representative z stacks of the superficial layers of the trunk of wild-type heterozygous and *xpr1b* mutant fish at 10 (D) and 21 dpf (E). Insets show representative images of Langerhans cells.

(F) Graph shows the average number of Langerhans cells in the field of view in the area of the trunk highlighted in the schematics.

Error bars show SEM. *$p \leq 0.05$, using paired two-tailed Student's t test (10 dpf siblings: n = 5, mutants n = 6; 21 dpf siblings: n = 7, mutants n = 6). Scale bar, 50 μm. See also Figure S4.

detected in the mutants (Figures 2B and 2E). In vivo time-lapse imaging of *mpeg1:EGFP*-labeled cells in the head showed that mutant macrophages divide at a rate similar to their wild-type counterparts (Figure S2; Movies S1 and S2), suggesting that reduced proliferation may not explain the decrease in the mutants. In addition, our in vivo time-lapse imaging analysis and TUNEL staining experiments showed no indication of higher cell death in mutant macrophages (Movies S1 and S2). Because the number of *mpeg1:EGFP*-expressing cells is reduced in the CNS of *xpr1b* mutants at 2 dpf, prior to the differentiation of microglia in the wild-type, and because no significant reduction in peripheral macrophages was found at this stage, the foregoing analyses suggest that migration and invasion of the brain by microglial precursors is reduced in *xpr1b* mutants.

The noncanonical NOD-like receptor *nlrc3-like* was recently reported to suppress inflammatory activation of primitive macrophages and to enable their migration and differentiation as microglia (Shiau et al., 2013). We sought to determine whether the migratory defect present in *xpr1b* mutants is related to that of *nlrc3-like* mutants. Similarly to *nlrc3-like* mutants, *xpr1b* mutants had higher than normal neutrophil numbers in the head. *xpr1b* mutants, however, did not have an increase of circulating neutrophils or increased levels of proinflammatory cytokines, which are characteristic of *nlrc3-like* mutants (Figure S3). Furthermore, Nlrc3-like expression did not rescue the microglia defect in *xpr1b* mutants, nor did Xpr1b expression rescue *nlrc3-like* mutants (Figure S3). These results provide evidence that *xpr1b* and *nlrc3-like* function in distinct genetic pathways that are essential for microglia formation in zebrafish.

xpr1b Mutant Macrophages Have Abnormal Morphology and Do Not Differentiate as Microglia

Although the number of microglial progenitors (macrophages located in the CNS) is reduced in *xpr1b* mutants, time-lapse imaging revealed that some *mpeg1:EGFP*-expressing cells are able to enter the brain parenchyma (Figure 2H; Movies S3 and S4). However, expression of the microglia marker *apoe* (Herbomel et al., 2001) was not observed in mutants at any stage examined (2.5 dpf, 5 dpf, and 10 dpf) (Figures 2G–2I). Furthermore, the morphology of *mpeg1:EGFP*-labeled cells was abnormal in *xpr1b* mutants. In *xpr1b* mutants at 3 dpf, about 72% of *mpeg1:EGFP*-labeled cells in the midbrain and hindbrain had no processes, compared to only 42% in wild-type (Figures 3A–3C). At 4 dpf, the morphological difference is even more pronounced, with the majority of cells having two or more processes in wild-type, whereas more than 60% of cells in the mutant had no processes (Figures 3A–C). These data indicate that *xpr1b* is required both for microglial progenitors to colonize the brain and also for these cells to differentiate into *apoe*-expressing, process-bearing microglia.

Number of Langerhans Cells and Their Complexity Is Affected in *xpr1b* Mutants

The requirement of *xpr1b* for the differentiation of primitive macrophages into microglia cells raised the possibility of this gene having a broader role in the differentiation of other specialized tissue macrophages. To examine this possibility, we analyzed Langerhans cells, a population of tissue macrophages that reside in the skin. In wild-type, the *mepg1:EGFP* transgene-labeled cells in the skin displayed many processes at 10 dpf and 21 dpf, consistent with the previously characterized location and morphology of Langerhans cells at these stages (Figures 3D and 3E) (Svahn et al., 2013). In *xpr1b* mutants, the number of these *mepg1:EGFP*-positive cells was reduced in the skin (Figure 3F), and the cells that were present had fewer processes (Figure S4). These results indicate that *xpr1b* is also essential for the normal development of Langerhans cells.

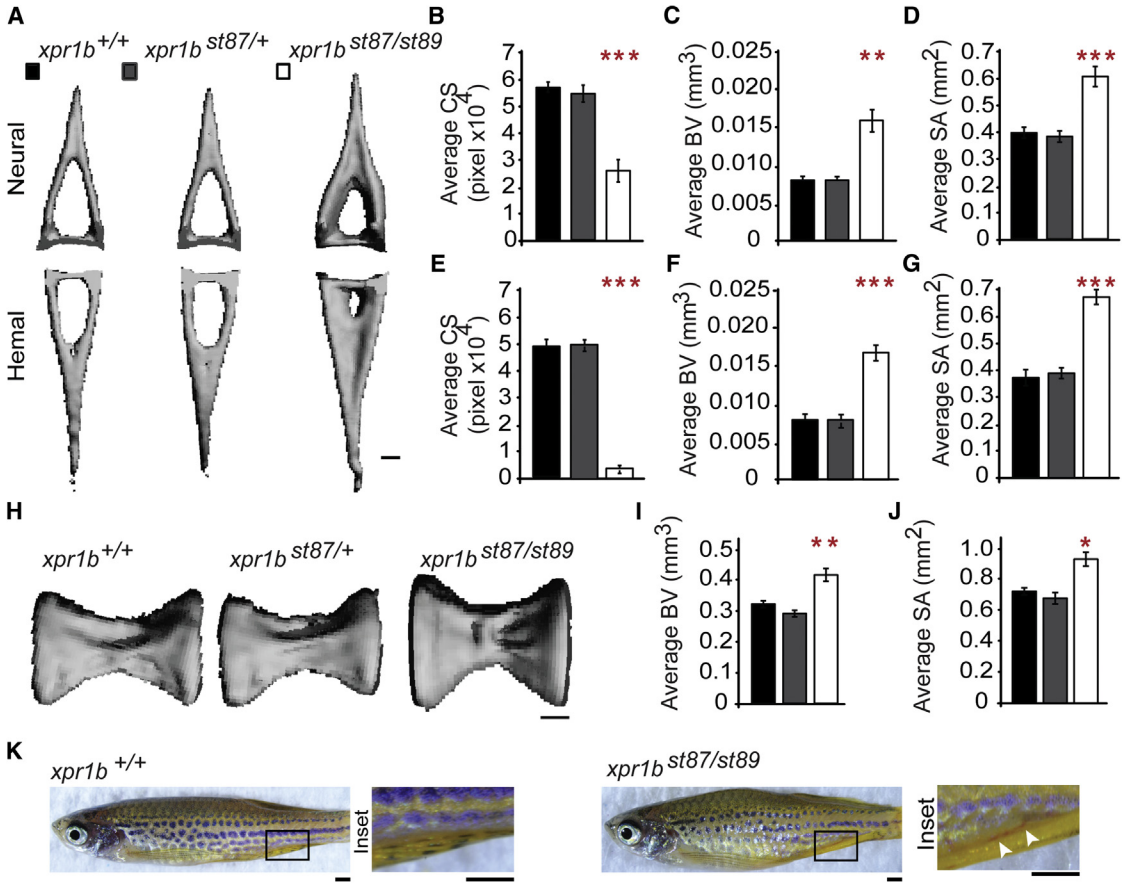

Figure 4. *xpr1b* Is Required for Normal Skeletal Development

(A) μCT-derived volumetric reconstructions of the neural (top) and hemal (bottom) 14th vertebral arches from a representative wild-type (n = 6), heterozygous (n = 7), and mutant (n = 6) fish. *xpr1b* mutant fish have excess bone on the inner surface of the arch compared to wild-type and heterozygous fish, reducing the overall aperture of the canal. Scale bar, 100 μm.

(B–G) Graphs showing quantified values for the vertebral arch defect depicted in (A). *xpr1b* mutant fish exhibit significant reductions in canal aperture (B and E) with a concomitant increase in the total amount of bone as measured by bone volume (BV; C and F) and surface area (SA; D and G).

(H) Volumetric reconstructions of the 14th vertebral bodies from a representative wild-type, heterozygous, and mutant fish. *xpr1b* mutant vertebral bodies appear larger than their wild-type and heterozygous siblings. Scale bar, 100 μm.

(I and J) Graphs depicting the significant increase in the total amount of bone present in mutant vertebrae as measured by BV (I) and SA (J). Error bars show SEM. Statistical significance was determined by unpaired, two-tailed t tests (*$p < 0.05$, **$p < 0.005$, ***$p < 5 \times 10^{-4}$).

(K) Lateral view of wild-type (left panel) and *xpr1b* mutant (right panel) adult fish. Inset shows the presence of an ectopic vessel in *xpr1b* mutants (right panel, arrowheads) that is absent in wild-type fish.

See also Figure S5.

xpr1b Mutants Have Impaired Bone Remodelling that Is Indicative of Osteoclast Defects

xpr1b mutants can survive to adulthood, although in reduced numbers compared to their siblings (Figure S5A). Furthermore, *xpr1b* mutants were also smaller than their siblings at 50 dpf but were able to continue growing (Figure S5B). Interestingly, some *xpr1b* mutant adults (two out of nine) displayed severe abnormalities in their body axis. In light of such severe malformations and reduced viability, we sought to determine whether Xpr1 is important for bone architecture. Micro-computed tomography (μCT) imaging revealed pronounced vertebral abnormalities in *xpr1b* mutants. Notably, the 14th and 16th hemal canals were about 10% of the wild-type size (Figures 4A and 4E; Figure S5). The neural canals of the same vertebrae were less affected in the mutants but still only about 40% of the wild-type size (Figures 4A and 4B; Figure S5). Likewise, *xpr1b* mutants had greater bone volumes and surface areas than their siblings (Figures 4A, 4C, 4D, 4F and 4G; Figure S5). These results suggest that in *xpr1b* mutants bone resorption is impaired. We extended our analysis to determine if the vertebral bodies of the 14th and 16th vertebrae also displayed features consistent with a defect in bone resorption. As with the vertebral arches, we found that *xpr1b* mutant vertebrae had greater bone volumes (Figures 4H and 4I) and surface areas (Figures 4H and 4J) than their siblings. These results are also consistent with a generalized defect in bone resorption in *xpr1b* mutants. Osteoclasts are cells derived from macrophages that have the primary function of resorbing bone during remodelling, and mutations that

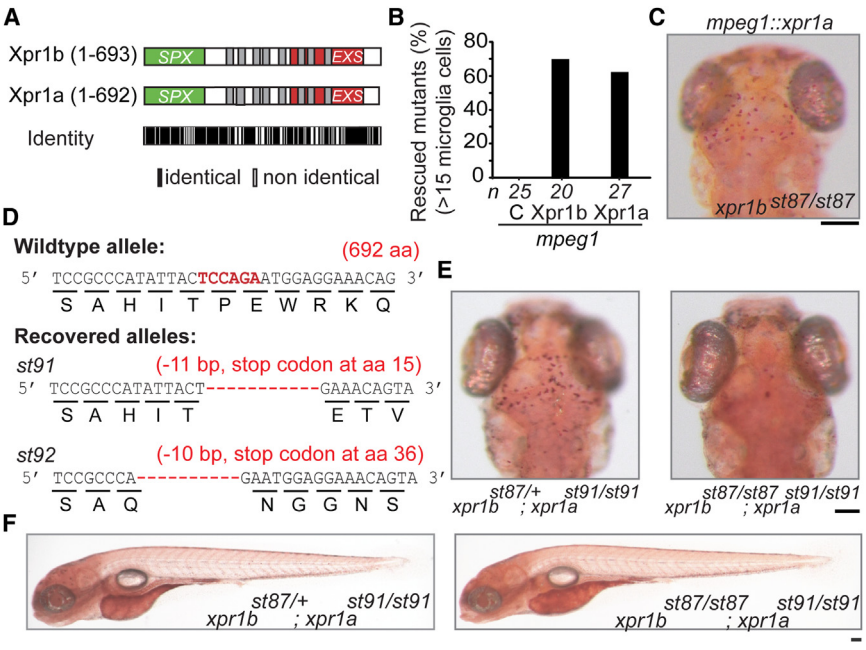

Figure 5. *xpr1a* Encodes a Functional Phosphate Exporter but Is Not Required for Microglia Development or Embryonic Development

(A) Graphic representation of the domain structure of Xpr1b and Xpr1a showing their shared identity.

(B) Graph representing the percentage of rescued *xpr1b* mutants when *xpr1b*, control *mcherry* (C), or *xpr1a* are expressed in the macrophage lineage.

(C) Representative dorsal image of a neutral red-stained 5 dpf *xpr1b* mutant larva rescued by expression of *xpr1a* in the macrophage lineage.

(D) Top panel shows diagram depicting the TALE nuclease targeted nucleotide sequence and the corresponding amino acid sequence of *xpr1a*. Bottom panels show the two alleles generated that have frameshift mutations in *xpr1a* coding sequence resulting in premature stop codons.

(E) Dorsal views of neutral red-stained 5 dpf *xpr1a* mutant (left) and *xpr1b;xpr1a* double mutant (right) show that *xpr1a* mutants have a normal number of microglia cells.

(F) Lateral views of neutral red-stained 5 dpf *xpr1a* mutant (left) and *xpr1b;xpr1a* double mutant (right) show grossly normal development at 5 dpf.

Scale bar, 50 μm.

affect osteoclasts number and function disrupt bone remodelling (Segovia-Silvestre et al., 2009). Indeed, the zebrafish *panther* mutant, which has a mutation in the macrophage colony-stimulating factor 1 receptor a (*csf1ra*), has a reduced number of osteoclasts and narrower neural and hemal canals due to increased bone mass (Chatani et al., 2011). Interestingly, *csfr1a* mutants also had impaired blood vessel formation, with the formation of an ectopic blood vessel that bypassed the occluded hemal canals. *xpr1b* mutants also had blood vessels in their ventral regions that were not observed in their siblings (Figure 4K). The parallels between *xpr1b* and *csfr1a* mutant phenotypes suggest that the skeletal defects in *xpr1b* mutants arise from a reduction of osteoclast number or function. Taken together, these phenotypic studies provide evidence that Xpr1 is essential for the development and function of diverse tissue macrophage populations, including microglia, Langerhans cells, and osteoclasts.

xpr1a, the Only Zebrafish Paralog of *xpr1b*, Is Not Required for Microglia or Normal Embryonic Development

The zebrafish genome contains a second *XPR1* homolog, *xpr1a*. Xpr1a shares 80% identity and 89% similarity with human XPR1 and 80% identity and 87% similarity with Xpr1b (Figure 5A). To investigate the function of *xpr1a*, we used TALE nucleases to generate mutations near the 5′ end of *xpr1a* coding sequence (Figure 5D). Homozygous mutants for two different frameshift mutations in *xpr1a* (*st91* and *st92*) had normal microglia development and gross embryonic morphology (Figures 5E and 5F and unpublished data). *xpr1a* homozygous mutants were viable as adults. Additionally, *xpr1b; xpr1a* double mutants resembled *xpr1b* single mutants, with reduced microglia but otherwise normal morphology in the embryo and early larva. Despite the evidence that XPR1 is the main phosphate exporter in metazoans, our genetic studies indicate the function of Xpr1 is required in specific cell types, including at least several macrophage lineages, and not broadly across all tissues.

Transgenic Expression of Xpr1a Rescues Microglia in *xpr1b* Mutants

To test if Xpr1a can functionally substitute for Xpr1b, we injected the progeny of an *xpr1b* heterozygous intercross with a transgene expressing *xpr1a* under the control of the macrophage lineage promoter, *mpeg1*. Expression of Xpr1a in the macrophage lineage rescued *xpr1b* mutants to similar levels as expression of Xpr1b (63% rescue with Xpr1a [n = 27] versus 69% rescue with Xpr1b [n = 20]; Figures 5B and 5C). Although zygotic *xpr1a* is not required for normal development, these results indicate that Xpr1a can fulfill the function of Xpr1b when expressed in the macrophage lineage.

DISCUSSION

XPR1, initially identified as a receptor for xenotropic and polytropic gamma retroviruses, is the only known phosphate exporter in metazoans (Giovannini et al., 2013). This multipass transmembrane protein is highly conserved across evolution, and closely related proteins are present in species as diverse as humans, plants, and unicellular eukaryotes. Previous analysis suggested that Xpr1 mediates phosphate export in a wide range of vertebrate cell types (Giovannini et al., 2013), but prior genetic studies did not analyze the role of Xpr1 in vertebrates in vivo. Our genetic analysis in zebrafish provides strong evidence that Xpr1b has a unique and specific function in highly specialized tissue-resident macrophages, including microglia and osteoclasts.

Phosphate Homeostasis and Tissue Specificity

In light of the functional conservation of Xpr1 homologs among metazoans and in budding yeast, the cell-type specificity of Xpr1b is remarkable. Complex regulatory mechanisms control phosphate homeostasis in unicellular and multicellular organisms. In the latter, Pi homeostasis occurs both at the cellular and organismal level. Cellular phosphate influx largely relies on the presence of sodium-dependent phosphate transporters (Biber et al., 2013; Forster et al., 2013). Whereas some of these transporters are ubiquitously expressed (e.g., SLC20A1 and SLCA20A2), expression of others (e.g., SLC34) is almost exclusively restricted to certain tissues with critical function in regulating organismal phosphate levels, such as the small intestine and kidney (Biber et al., 2013; Forster et al., 2013). The expression and activity of these transporters are regulated by many factors to ensure that phosphate homeostasis is maintained.

The biochemical function of Xpr1 as a phosphate exporter was only recently described (Giovannini et al., 2013), and the role of phosphate exporters in organismal phosphate homeostasis remains elusive. Our data suggest that Xpr1b is not required for phosphate transport or other functions in most cell types but is instead required in a specific subset of cells, including microglia, Langerhans cells, and osteoclasts. Our analysis suggests that the regulated activity of sodium-dependent phosphate transporters is sufficient for proper phosphate balance in most cell types and that the requirement for dedicated phosphate exporters is restricted to cells that experience extreme phosphate fluctuations. Such cells could include highly phagocytic cells, including microglia, cells involved in phosphate (re)absorption (e.g., small intestine enterocytes and proximal tubule cells), and cells involved in bone resorption (osteoclasts). In fact, the presence of a dedicated phosphate exporter has long been hypothesized in epithelial renal cells and osteoclasts (Barac-Nieto et al., 2002; Ito et al., 2007). In particular, osteoclasts were shown to have a unique Pi efflux system, involved in the continuous release of Pi at the basolateral plasma membrane preventing accumulation of intracellular inorganic phosphate (Ito et al., 2007). In assays of cultured mammalian cells, Xpr1 mediates phosphate export (Giovannini et al., 2013), and our genetic studies indicate that Xpr1b has an essential function in osteoclasts and other tissue macrophages in vivo. To explore the possibility that *xpr1a*, which encodes a protein 80% identical to Xpr1b, might have functions overlapping with *xpr1b*, we used transgenic and mutational approaches. As one might expect from the extent of sequence similarity, our experiments indicate that a transgene expressing Xpr1a in the macrophage lineage restores microglia in *xpr1b* mutants. Nonetheless, *xpr1a* mutants were phenotypically indistinguishable from their wild-type siblings, and *xpr1b:xpr1a* double mutants were phenotypically similar to *xpr1b* single mutants. Therefore, it seems that the zygotic functions Xpr1b and Xpr1a are largely dispensable for the early development of many cell types. It is important to note that earlier functions, in and out of the macrophage lineage, might be masked by the maternal expression of both these proteins. Nevertheless, the double mutants survive for at least 20 days postfertilization, further supporting the possibility that these phosphate exporters have cell-type-specific rather than general functions.

Xpr1b and Development of Tissue-Resident Macrophages

The cytokine colony-stimulating factor 1 (CSF1), the interleukin IL-34, and their receptor, colony-stimulating factor 1 receptor (CSF1R), are key regulators of macrophage development (Davies et al., 2013; Wynn et al., 2013). Studies in mice, rats, and zebrafish have revealed a conserved role of the macrophage colony-stimulating factor 1 receptor a (*csfr1a* aka *fms*) in the establishment of many tissue-resident populations, including microglia, osteoclasts, and Langerhans cells (Droin and Solary, 2010; Nakamichi et al., 2013). In zebrafish, *csfr1a* mutants (*panther* mutants) have primitive macrophages, which proliferate and move but fail to colonize the brain and other target tissues (Herbomel et al., 2001). Similarly, migration of macrophages into the brain is reduced in *xpr1b* mutants. In contrast to *csfr1a*/*panther* mutants, in *xpr1b* mutants, the small number of macrophages that are able to enter the brain parenchyma do not differentiate into *apoe*-expressing microglia. In addition, in *xpr1b* mutants, there is no recovery of the microglia population as larval development begins, in contrast to *csfr1a*/*panther* mutant larvae, which gain increasing numbers of microglia as larval development progresses. *csfr1a*/*panther* and *xpr1b* mutants also share an osteopetrotic phenotype, which appears to be more severe in *xpr1b* mutants, as judged by the extent of occlusion of the neural and hemal canals. Although we did not experimentally address the autonomy of Xpr1b in Langerhans cells and osteoclasts, we have shown that Xpr1b acts autonomously in the macrophage lineage to rescue the microglia phenotype. Because Langerhans and osteoclasts are also derived in part from primitive macrophages (Ginhoux et al., 2010; Hoeffel et al., 2012), it is likely that Xpr1b acts autonomously not only in microglia but also in these other tissue macrophage populations. Further experiments are required to determine if there is any relationship between *xpr1b* and *csfr1a* signaling and to determine the mechanisms by which the loss of the phosphate exporter disrupts the establishment of tissue resident macrophage populations. It is also possible that XPR1 has other functions that are essential for development of tissue macrophages, in addition to its activity as a phosphate exporter (Giovannini et al., 2013; Wege and Poirier, 2014).

In summary, we show that the phosphate exporter Xpr1b acts specifically and autonomously in the macrophage lineage. Our analysis of *xpr1a* mutants and *xpr1b;xpr1a* double mutants shows that the zygotic function of this phosphate exporter is required only in specific cell types and not generally for development and survival of the larva. Our *xpr1a* and *xpr1b* mutants will be valuable in the analysis of the intricate regulation of phosphate homeostasis at the cellular and organismal level in vivo.

EXPERIMENTAL PROCEDURES

Zebrafish Lines and Embryos

Wild-type (TL, AB/TU, and WK), transgenic, and heterozygous *xpr1b* fish were raised at 28.5°C and staged as described previously (Kimmel et al., 1995). To inhibit pigmentation, embryos were treated with 0.003% 1-phenyl-2-thiourea (PTU) in methylene blue embryo water. The transgenic lines *Tg(lyz:EGFP)*, *Tg(mpeg1:EGFP)*, and *Tg(kdrl:mCherry-CAAX)* have been previously described (Hall et al., 2007; Ellett et al., 2011; Fujita et al., 2011). Experimental

protocols involving zebrafish were approved by the Stanford University Institutional Animal Care and Use Committee.

ENU Mutagenesis, Microglia Screen, and Neutral Red Assay

Founder P0 wild-type males were mutagenized with ENU and subsequently outcrossed to raise F1 and F2 families for screening as described previously (Pogoda et al., 2006). An F3 genetic screen was conducted to identify putative mutants with specific defects in microglia (e.g., loss of microglia) but no apparent anatomical morphological defects at 5 dpf. Microglial cells were scored in live 3–5 dpf larvae after treatment with the vital dye neutral red as described previously (Shiau et al., 2013). Briefly, larvae were incubated in embryo water containing 2.5 μg/ml neutral red at 28.5°C for 2–3 hr, followed by two water changes, and analyzed 4–24 hr later using a dissection microscope.

Genetic Mapping

st87 mutant embryos were separated from wild-type siblings based on the neutral red phenotype, lack of microglia, at 5 dpf. Bulk segregant analysis with 480 simple sequence-length polymorphisms (SSLPs) (Pogoda et al., 2006) identified markers on LG2 flanking the *st87* mutation. High-resolution mapping was conducted using additional SSLPs and SNPs linked to the mutation, which were found from sequencing PCR fragments amplified from genomic DNA of mutants and wild-type siblings. Sequencing of PCR products of genes in the critical interval identified *st87* lesion in the *xpr1b* gene. *st87* lesion was genotyped based on the PCR/restriction digest assay using the forward primer (5′-GCTGCTAACAGAATACTTCCT-3′), reverse primer (5′-CCAGTCCCGGCTTGGACTCTGA-3′), and digestion with DdeI.

Sequence-Specific TALE Nucleases

The 5′ regions of *xpr1b* and *xpr1a* genes were selected as targets. The web tool TAL Effector-Nucleotide Targeter 2.0 (TALE-NT 2.0; https://tale-nt.cac.cornell.edu) was used to design transcription activator-like effector nuclease (TALEN) pairs and identify a diagnostic restriction enzyme. The specific sequence for each TALEN is detailed in Table S1. TALEN assembly followed the PCR/Golden Gate cloning protocol (Sanjana et al., 2012). TALE nuclease mRNA was transcribed using the Sp6 mMessage mMachine kit (Ambion). A total of 400–800 pg of TALE nuclease mRNA was injected into one- to two-cell-stage embryos, which were raised at 28.5°C. Carriers of deletions in the *xpr1b* and *xpr1a* genes were identified by PCR/restriction digest assay with the primers present in Table S1 and the restriction enzymes FspI and Hpy188III. Stable lines of two different alleles for each gene were established.

Whole-Mount In Situ Hybridization

In situ hybridization on whole zebrafish embryos and larvae was performed as previously described (Pogoda et al., 2006). Antisense riboprobes were transcribed for *lyz*, *mfap4, apoe*, and *mpx* as described previously (Shiau et al., 2013).

Time-Lapse and Fluorescent Imaging

Embryos and larvae used for live imaging were treated with 0.016% (w/v) tricaine, mounted in 1.5% low-melting-point agarose, and imaged at room temperature. Images for determination of average number of *mpeg1:EGFP*-positive cells were acquired on a Zeiss Axio Observer microscope coupled to a Perkin Elmer UltraView vox spinning-disk confocal. Images of laterally mounted embryos and larvae were captured with a Hamamatsu camera, using the Volocity Acquisition suite for multidimensional multichannel time-lapse recording. Images were analyzed using Volocity software and processed with Adobe Photoshop. All other imaging was done on a Zeiss LSM 5 Pascal confocal microscope. Image J software was used to make maximum intensity projections of z stacks, and images were processed for contrast and brightness in Photoshop. The average number of Langerhans cells was determined by counting the number of *mpeg1:EGFP*-positive cells present in the skin in the field of view. Images were taken always from the region immediately posterior to the anal fin. Analysis of the number of projections per cell was done per field of view and in maximum-intensity projections obtained using ImageJ software. Time-lapse imaging of *mpeg1:EGFP; kdrl:mcherryCAAX* transgenic line was done by capturing one z stack per 20 s for 30 min, using the 20× objective.

Expression Constructs

The coding sequences of *xpr1b and xpr1b* were cloned from a 5 dpf embryonic cDNA pool and directionally inserted into pCR8/GW/TOPO vector (Invitrogen); primers used are in Table S1. For RNA expression, *xpr1b* sequence was subcloned into the pCSDest vector using multsite GATEWAY technology (Kwan et al., 2007). Tol2 sequence containing constructs used for tissue-specific expression were also made using multisite GATEWAY (Kwan et al., 2007). The tissue-specific regulatory sequences used have been reported elsewhere (Shiau et al., 2013). Tissue-specific transgenes were transiently expressed by coinjecting 12–25 pg of Tol2-plasmids described above and 100–200 pg of Tol2 transposase mRNA into one-cell embryos.

Bone-Remodeling Phenotypes

Wild-type ($xpr1b^{+/+}$, n = 6), heterozygous ($xpr1b^{st87/+}$ and $xpr1b^{st89/+}$, n = 3 and n = 4, respectively), and mutant fish ($xpr1b^{st87/st89}$, n = 6) were collected when their standard length was 2.5 cm, fixed in 4% paraformaldehyde for 24 hr, and rinsed in 1× PBS. Skeletal phenotypes were evaluated by μCT. Fish were scanned in 1× PBS using a Scanco μCT40 operated at 70 kVp, 114 μA, at medium resolution, and with 2× averaging. Voxel size was 12 μm^3 for all fish. Evaluation of the 14th and 16th vertebral arches was performed on an average of 63 (hemal) and 65 (neural) 2D slices (~750–780 μm) beginning at the anterior edge of each arch. Volumetric reconstruction images were imported into Adobe Photoshop and measured to determine the average canal aperture for each genotypic class (defined as the total number of pixels corresponding to the arch opening). Bone volume (direct) and surface area (TRI-plate model) measurements were evaluated using Scanco/OpenVMS software. Characterization of vertebral body defects of the 14th and 16th vertebrae was performed by evaluation of an average of 53 2D slices (~640 μm) beginning at the anterior edge of each vertebra. Bone volume and surface area measurements were determined as above. Statistical significance of all measurements was determined by unpaired, two-tailed t tests.

SUPPLEMENTAL INFORMATION

Supplemental Information includes Supplemental Experimental Procedures, five figures, one table, and four movies and can be found with this article online at http://dx.doi.org/10.1016/j.celrep.2014.08.018.

AUTHOR CONTRIBUTIONS

A.M.M. mapped the *st87* mutation; generated *st89*, *st90*, *st91*, and *st92*; and conducted all experiments on *xpr1b* and *xpr1a* mutants. C.E.S., H.S., A.M.M., and W.S.T. performed the genetic screen. C.E.S. analyzed the genetic interaction of *nlrc3-like* and *xpr1b*. C.A.G. and D.M.K. performed all the analysis of bone development. A.M.M. and W.S.T. analyzed the data and wrote the manuscript, with input from all the authors.

ACKNOWLEDGMENTS

We are grateful to M. Barna and S. Kim for sharing equipment. Special thanks to Talbot lab members for critical comments on the manuscript and T. Reyes and C. Hill for fish care. A.M.M. was supported by EMBO fellowship ALTF 1125-2011. C.E.S. was supported by NIH NRSA fellowship 5F32NS067754, and H. S. was supported by an A*STAR fellowship. D.M.K. is an investigator of the Howard Hughes Medical Institute. C.A.G. is supported by HHMI. This work was supported by NIH grant R01 NS065787 to W.S.T.

Received: May 26, 2014
Revised: July 23, 2014
Accepted: August 8, 2014
Published: September 11, 2014

REFERENCES

Barac-Nieto, M., Alfred, M., and Spitzer, A. (2002). Basolateral phosphate transport in renal proximal-tubule-like OK cells. Exp. Biol. Med. (Maywood) *227*, 626–631.

Battini, J.L., Rasko, J.E., and Miller, A.D. (1999). A human cell-surface receptor for xenotropic and polytropic murine leukemia viruses: possible role in G protein-coupled signal transduction. Proc. Natl. Acad. Sci. USA *96*, 1385–1390.

Begg, S.K., Radley, J.M., Pollard, J.W., Chisholm, O.T., Stanley, E.R., and Bertoncello, I. (1993). Delayed hematopoietic development in osteopetrotic (op/op) mice. J. Exp. Med. *177*, 237–242.

Biber, J., Hernando, N., and Forster, I. (2013). Phosphate transporters and their function. Annu. Rev. Physiol. *75*, 535–550.

Chatani, M., Takano, Y., and Kudo, A. (2011). Osteoclasts in bone modeling, as revealed by in vivo imaging, are essential for organogenesis in fish. Dev. Biol. *360*, 96–109.

Christian, M., Cermak, T., Doyle, E.L., Schmidt, C., Zhang, F., Hummel, A., Bogdanove, A.J., and Voytas, D.F. (2010). Targeting DNA double-strand breaks with TAL effector nucleases. Genetics *186*, 757–761.

Davies, L.C., Jenkins, S.J., Allen, J.E., and Taylor, P.R. (2013). Tissue-resident macrophages. Nat. Immunol. *14*, 986–995.

Droin, N., and Solary, E. (2010). Editorial: CSF1R, CSF-1, and IL-34, a "menage a trois" conserved across vertebrates. J. Leukoc. Biol. *87*, 745–747.

Ellett, F., Pase, L., Hayman, J.W., Andrianopoulos, A., and Lieschke, G.J. (2011). mpeg1 promoter transgenes direct macrophage-lineage expression in zebrafish. Blood *117*, e49–e56.

Forster, I.C., Hernando, N., Biber, J., and Murer, H. (2013). Phosphate transporters of the SLC20 and SLC34 families. Mol. Aspects Med. *34*, 386–395.

Fujita, M., Cha, Y.R., Pham, V.N., Sakurai, A., Roman, B.L., Gutkind, J.S., and Weinstein, B.M. (2011). Assembly and patterning of the vascular network of the vertebrate hindbrain. Development *138*, 1705–1715.

Ginhoux, F., Greter, M., Leboeuf, M., Nandi, S., See, P., Gokhan, S., Mehler, M.F., Conway, S.J., Ng, L.G., Stanley, E.R., et al. (2010). Fate mapping analysis reveals that adult microglia derive from primitive macrophages. Science *330*, 841–845.

Giovannini, D., Touhami, J., Charnet, P., Sitbon, M., and Battini, J.L. (2013). Inorganic phosphate export by the retrovirus receptor XPR1 in metazoans. Cell Reports *3*, 1866–1873.

Hall, C., Flores, M.V., Storm, T., Crosier, K., and Crosier, P. (2007). The zebrafish lysozyme C promoter drives myeloid-specific expression in transgenic fish. BMC Dev. Biol. *7*, 42.

Herbomel, P., Thisse, B., and Thisse, C. (2001). Zebrafish early macrophages colonize cephalic mesenchyme and developing brain, retina, and epidermis through a M-CSF receptor-dependent invasive process. Dev. Biol. *238*, 274–288.

Hoeffel, G., Wang, Y., Greter, M., See, P., Teo, P., Malleret, B., Leboeuf, M., Low, D., Oller, G., Almeida, F., et al. (2012). Adult Langerhans cells derive predominantly from embryonic fetal liver monocytes with a minor contribution of yolk sac-derived macrophages. J. Exp. Med. *209*, 1167–1181.

Ito, M., Haito, S., Furumoto, M., Uehata, Y., Sakurai, A., Segawa, H., Tatsumi, S., Kuwahata, M., and Miyamoto, K. (2007). Unique uptake and efflux systems of inorganic phosphate in osteoclast-like cells. Am. J. Physiol. Cell Physiol. *292*, C526–C534.

Kimmel, C.B., Ballard, W.W., Kimmel, S.R., Ullmann, B., and Schilling, T.F. (1995). Stages of embryonic development of the zebrafish. Dev. Dyn. *203*, 253–310.

Kwan, K.M., Fujimoto, E., Grabher, C., Mangum, B.D., Hardy, M.E., Campbell, D.S., Parant, J.M., Yost, H.J., Kanki, J.P., and Chien, C.B. (2007). The Tol2kit: a multisite gateway-based construction kit for Tol2 transposon transgenesis constructs. Dev. Dyn. *236*, 3088–3099.

Nakamichi, Y., Udagawa, N., and Takahashi, N. (2013). IL-34 and CSF-1: similarities and differences. J. Bone Miner. Metab. *31*, 486–495.

Paolicelli, R.C., Bolasco, G., Pagani, F., Maggi, L., Scianni, M., Panzanelli, P., Giustetto, M., Ferreira, T.A., Guiducci, E., Dumas, L., et al. (2011). Synaptic pruning by microglia is necessary for normal brain development. Science *333*, 1456–1458.

Peri, F., and Nüsslein-Volhard, C. (2008). Live imaging of neuronal degradation by microglia reveals a role for v0-ATPase a1 in phagosomal fusion in vivo. Cell *133*, 916–927.

Pogoda, H.M., Sternheim, N., Lyons, D.A., Diamond, B., Hawkins, T.A., Woods, I.G., Bhatt, D.H., Franzini-Armstrong, C., Dominguez, C., Arana, N., et al. (2006). A genetic screen identifies genes essential for development of myelinated axons in zebrafish. Dev. Biol. *298*, 118–131.

Pollard, J.W. (1997). Role of colony-stimulating factor-1 in reproduction and development. Mol. Reprod. Dev. *46*, 54–60, discussion 60–61.

Ransohoff, R.M., and Cardona, A.E. (2010). The myeloid cells of the central nervous system parenchyma. Nature *468*, 253–262.

Sanjana, N.E., Cong, L., Zhou, Y., Cunniff, M.M., Feng, G., and Zhang, F. (2012). A transcription activator-like effector toolbox for genome engineering. Nat. Protoc. *7*, 171–192.

Schafer, D.P., Lehrman, E.K., Kautzman, A.G., Koyama, R., Mardinly, A.R., Yamasaki, R., Ransohoff, R.M., Greenberg, M.E., Barres, B.A., and Stevens, B. (2012). Microglia sculpt postnatal neural circuits in an activity and complement-dependent manner. Neuron *74*, 691–705.

Secco, D., Wang, C., Arpat, B.A., Wang, Z., Poirier, Y., Tyerman, S.D., Wu, P., Shou, H., and Whelan, J. (2012a). The emerging importance of the SPX domain-containing proteins in phosphate homeostasis. New Phytol. *193*, 842–851.

Secco, D., Wang, C., Shou, H., and Whelan, J. (2012b). Phosphate homeostasis in the yeast Saccharomyces cerevisiae, the key role of the SPX domain-containing proteins. FEBS Lett. *586*, 289–295.

Segovia-Silvestre, T., Neutzsky-Wulff, A.V., Sorensen, M.G., Christiansen, C., Bollerslev, J., Karsdal, M.A., and Henriksen, K. (2009). Advances in osteoclast biology resulting from the study of osteopetrotic mutations. Hum. Genet. *124*, 561–577.

Shiau, C.E., Monk, K.R., Joo, W., and Talbot, W.S. (2013). An anti-inflammatory NOD-like receptor is required for microglia development. Cell Reports *5*, 1342–1352.

Svahn, A.J., Graeber, M.B., Ellett, F., Lieschke, G.J., Rinkwitz, S., Bennett, M.R., and Becker, T.S. (2013). Development of ramified microglia from early macrophages in the zebrafish optic tectum. Dev. Neurobiol. *73*, 60–71.

Tailor, C.S., Nouri, A., Lee, C.G., Kozak, C., and Kabat, D. (1999). Cloning and characterization of a cell surface receptor for xenotropic and polytropic murine leukemia viruses. Proc. Natl. Acad. Sci. USA *96*, 927–932.

Vaughan, A.E., Mendoza, R., Aranda, R., Battini, J.L., and Miller, A.D. (2012). Xpr1 is an atypical G-protein-coupled receptor that mediates xenotropic and polytropic murine retrovirus neurotoxicity. J. Virol. *86*, 1661–1669.

Wege, S., and Poirier, Y. (2014). Expression of the mammalian Xenotropic Polytropic Virus Receptor 1 (XPR1) in tobacco leaves leads to phosphate export. FEBS Lett. *588*, 482–489.

Wynn, T.A., Chawla, A., and Pollard, J.W. (2013). Macrophage biology in development, homeostasis and disease. Nature *496*, 445–455.

Yang, Y.L., Guo, L., Xu, S., Holland, C.A., Kitamura, T., Hunter, K., and Cunningham, J.M. (1999). Receptors for polytropic and xenotropic mouse leukaemia viruses encoded by a single gene at Rmc1. Nat. Genet. *21*, 216–219.

Zakrzewska, A., Cui, C., Stockhammer, O.W., Benard, E.L., Spaink, H.P., and Meijer, A.H. (2010). Macrophage-specific gene functions in Spi1-directed innate immunity. Blood *116*, e1–e11.